

# Petroleum Crude Oil Characterization by IMS-MS and FTICR MS

Francisco A. Fernandez-Lima,<sup>†</sup> Christopher Becker,<sup>‡</sup> Amy M. McKenna,<sup>§</sup> Ryan P. Rodgers,<sup>§,II</sup> Alan G. Marshall,<sup>§,II</sup> and David H. Russell\*,<sup>†</sup>

Department of Chemistry, Texas A&M University, College Station, Texas 77843, Department of Chemistry, Baylor University, Waco, Texas 76706, Ion Cyclotron Resonance Program, National High Magnetic Field Laboratory, Florida State University, 1800 East Paul Dirac Drive, Tallahassee, Florida 32310-4005, and Department of Chemistry & Biochemistry, Florida State University, Tallahassee, Florida 32306

Here, complementary ion mobility/mass spectrometry (IM/MS) and ultrahigh-resolution Fourier transform ion cyclotron resonance (FTICR) MS analyses of light, medium, and heavy petroleum crude oils yielded distributions of the heteroatom-containing hydrocarbons, as well as multiple conformational classes. The IM/MS technique provides unique fingerprints for fast identification of signature conformational/compositional patterns, whereas FTICR MS analysis provides comprehensive heteroatom class distributions. IM/MS and FTICR MS results reveal an increase in compositional complexity in proceeding from light to medium to heavy crude oils. Inspection of the mobility results shows a high structural diversity for the  $C_nH_nXY$  ( $XY = N_1, S_1, N_1, O_1, NS, SO_{1-2}, NO_{1-2}$ , etc.) series, as well as a shift from planar to more compact three-dimensional structures with increasing mass.

Petroleum crude oils are complex mixtures containing tens of thousands of chemically distinct organic compositions within a dynamic range of 10000–100000 in relative abundance. Current technical and industrial applications of petroleum crude oil and its products demand fast and accurate chemical fingerprinting of hydrocarbons, specifically, noncovalent multimers and distributions of heteroatoms, rings, and double bonds. That information can, in turn, potentially determine the characteristics of the refining process and the production efficiency to convert the full mass balance into useful energy and ultimately the economic value of the petroleum crude oil and the level of environmental pollution upon combustion (e.g.,  $NO_x$  and  $SO_x$  emissions).

Identification and quantification of a limited number of a priori selected compounds have been used for oil spill identification.<sup>1</sup> Although characteristic crude oil features have been observed by infrared and near-infrared spectroscopy, bulk sample measurements cannot resolve individual compounds in crude oils.<sup>2</sup>

\* To whom correspondence should be addressed. E-mail: russell@mail.chem.tamu.edu.

<sup>†</sup> Texas A&M University.

<sup>‡</sup> Baylor University.

<sup>§</sup> Florida State University.

<sup>II</sup> National High Magnetic Field Laboratory.

(1) Daling, P. S.; Faksness, L. G.; Hansen, A. B.; Stout, S. A. *Environ. Forensics* 2002, 3, 263–278.

(2) Aske, N.; Kallevic, H.; Sjöblom, J. *Energy Fuels* 2001, 15, 1304–1312.

Chromatographic separations and curve deconvolution is problematic for oils and petroleum products, mainly because the number of elemental compositions and isomers becomes enormous for compounds containing 20 or more carbons. Moreover, gas chromatography/mass spectrometry (GC/MS<sup>3</sup> and GC/GC/MS<sup>4</sup>) cannot access heavy-ends species (with boiling points of >400–450 °C). Fourier transform ion cyclotron resonance (FTICR) MS can identify the elemental composition, double bond equivalents (DBE = rings plus double bonds to carbon), and carbon number, based on ultra-high-resolution and accurate mass measurements.<sup>5–8</sup> A critical issue for the analysis of crude oils and asphaltenes is the degree of aggregation, as recently comprehensively reviewed.<sup>9</sup> Noncovalent aggregates can be minimized in electrospray ionization (ESI) and atmospheric-pressure photoionization (APPI), but can be prominent in single-photon (but not two-photon<sup>10</sup>) laser desorption ionization.

Ion mobility/mass spectrometry (IM/MS) is a post-ionization separation method that adds size and shape dimensions to MS. That is, ions are separated as they drift in a bath gas under the influence of an external electric field; thus, separation is based on the ion–neutral collision cross section on a millisecond time scale. The coupling of IMS and MS has shown a unique strength in the identification of peptide and protein secondary structures;<sup>11–17</sup>

- (3) Zadro, S.; Haken, J. K.; Pinczewski, W. V. *J. Chromatogr.* 1985, 323, 305–322.
- (4) Wang, F. C. Y.; Wan, K. N.; Green, L. A. *Anal. Chem.* 2005, 77, 2777–2785.
- (5) Marshall, A. G.; Hendrickson, C. L.; Jackson, G. S. *Mass Spectrom. Rev.* 1998, 17, 1–35.
- (6) Marshall, A. G.; Rodgers, R. P. *Acc. Chem. Res.* 2004, 37, 53–59.
- (7) Marshall, A. G.; Rodgers, R. P. *Proc. Natl. Acad. U.S.A.* 2008, 105, 18090–18095.
- (8) Rodgers, R. P.; Schaub, T. M.; Marshall, A. G. *Anal. Chem.* 2005, 77, 20A–27A.
- (9) Soraya, S.; Betancourt, S. S.; Ventura, G. T.; Pomerantz, A. E.; Viloria, O.; Dubost, F. X.; Zuo, J.; Monson, G.; Bustamante, D.; Purcell, J. M.; Nelson, R. K.; Rodgers, R. P.; Reddy, C. M.; Marshall, A. G.; Mullins, O. C. *Energy Fuels* 2009, 23, 1178–1188.
- (10) Pomerantz, A. E.; Hammond, M. R.; Morrow, A. L.; Mullins, O. C.; Zare, R. N. *Energy Fuels* 2009, 23, 1162–1168.
- (11) Wyttenbach, T.; von Helden, G.; Bowers, M. T. *J. Am. Chem. Soc.* 1996, 118, 8355–8364.
- (12) Hudgins, R. R.; Woenckhaus, J.; Jarrold, M. F. *Int. J. Mass Spectrom. Ion Processes* 1997, 165–166, 497–507.
- (13) Valentine, S. J.; Counterman, A. E.; Hoaglund, C. S.; Reilly, J. P.; Clemmer, D. E. *J. Am. Soc. Mass Spectrom.* 1998, 9, 1213–1216.
- (14) Sawyer, H. A.; Marini, J. T.; Stone, E. G.; Ruotolo, B. T.; Gillig, K. J.; Russell, D. H. *J. Am. Soc. Mass Spectrom.* 2005, 16, 893–905.

alkali halide<sup>17,18</sup> and carbon clusters,<sup>19,20</sup> polymeric molecules,<sup>21</sup> and more recently, the gas-phase aggregates produced by ionization of asphaltenes and deasphaltenes oils.<sup>22</sup> Here, the combined determination of size/shape (IM/MS) and organic composition (APPI FTICR MS) connects the conformational and chemical characterization of petroleum crude oils.

## SAMPLE PREPARATION

Three samples of petroleum crude oils were used as received without further purification prior to laser desorption/ionization (LDI)/IM/MS analysis (courtesy of Professor Dr. Daulat D. Mamora, Department of Petroleum Engineering, Texas A&M University). Samples correspond to the Calvert, Duri, and San Andro extraction regions and are classified as light, medium, and heavy crude oils, respectively. For the San Andro crude oil, the *n*-heptane-soluble and -insoluble fractions were separated by vacuum filtration with a glass frit. For the ultra-high-resolution MS analysis, the crude oils were diluted in toluene to a final concentration of 500 µg/mL prior to analysis.

## INSTRUMENTATION

The LDI/IM/TOF mass spectrometer was described previously (see scheme in Figure 1).<sup>23–27</sup> Briefly, ions are formed in an IM drift cell by irradiating the sample plate with the output from a microcrystal Nd:YAG laser (355 nm, Powerchip Nanolaser, JDS Uniphase Corp.). In the IM drift cell, ions are separated on the basis of ion–neutral collision cross sections; typical operating conditions are 3 Torr of helium buffer gas and field strength/pressure ratios of 10–35 V cm<sup>−1</sup> torr<sup>−1</sup>. The IM drift cell consists of a stacked-ring ion guide design,<sup>24,27</sup> where electrode pairs are spaced 1.5 mm apart and the spacing between the electrode pairs is 3.0 mm. Subsequent electrodes are connected via a resistor divider network composed of 1 MΩ resistors. Ions exiting the IM drift cell are focused (by a multielement Einzel lens) into the orthogonal TOF ion source. The TOF tube is biased at a potential of −6 kV, and the ions are extracted by applying a voltage pulse to the TOF push/pull electrodes (+675 V/−675 V, respectively);

- (15) Ruotolo, B. T.; Tate, C. C.; Russell, D. H. *J. Am. Soc. Mass Spectrom.* **2004**, *15*, 870–878.
- (16) Tao, L.; McLean, J. R.; McLean, J. A.; Russell, D. H. *J. Am. Soc. Mass Spectrom.* **2007**, *18*, 1232–1238.
- (17) Fernandez-Lima, F. A.; Wei, H.; Gao, Y. Q.; Russell, D. H. *J. Phys. Chem. A* **2009**, *113*, 8221–8234.
- (18) Dugourd, P.; Hudgins, R. R.; Jarrold, M. F. *Chem. Phys. Lett.* **1997**, *267*, 186–192.
- (19) von Helden, G.; Hsu, M.; Kemper, P. R.; Bowers, M. T. *J. Chem. Phys.* **1991**, *95*, 3835–3837.
- (20) Scott, C. D.; Ugarov, M.; Hauge, R. H.; Sosa, E. D.; Arepalli, S.; Schultz, J. A.; Yowell, L. *J. Phys. Chem. C* **2007**, *111*, 36–44.
- (21) Jackson, A. T.; Scrivens, J. H.; Williams, J. P.; Baker, E. S.; Gidden, J.; Bowers, M. T. *Int. J. Mass Spectrom.* **2004**, *238*, 287–297.
- (22) Becker, C.; Qian, K.; Russell, D. H. *Anal. Chem.* **2008**, *80*, 8592–8597.
- (23) Koomen, J. M.; Ruotolo, B. T.; Gillig, K. J.; McLean, J. A.; Russell, D. H.; Kang, M.; Dunbar, K. R.; Fuhrer, K.; Gonin, M.; Schultz, J. A. *Anal. Bioanal. Chem.* **2002**, *373*, 612–617.
- (24) Fuhrer, K.; Gonin, M.; Schultz, J. A. U.S. Patent Application US20050189486, 2005.
- (25) Raznikov, V. V.; Schultz, J. A.; Egan, T. F.; Ugarov, M. V.; Tempez, A.; Savenkov, G.; Zelenov, V. (Ionwerks, Inc.) International Patent Application WO2006130475, 2006.
- (26) Gillig, K. J.; Ruotolo, B.; Stone, E. G.; Russell, D. H.; Fuhrer, K.; Gonin, M.; Schultz, J. A. *J. Anal. Chem.* **2000**, *72*, 3965–3971.
- (27) Schultz, J. A.; Raznikov, V.; Egan, T. F.; Ugarov, M. V.; Tempez, A. U.S. Patent Application US00722396B2, 2007.

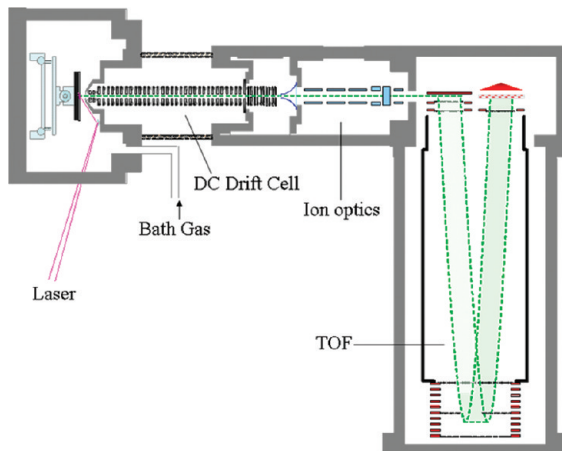


**Figure 1.** Schematic diagram of the IM/MS instrument, including an LDI source, a periodic drift cell, and a reflectron orthogonal TOF tube.

the TOF extraction potential is pulsed at 10–20 kHz, and the typical mass resolving power,  $m/\Delta m_{50\%}$  in which  $\Delta m_{50\%}$  is the peak full width at half-maximum peak height, for the reflectron TOF setup is 2500–3000. The IM/MS spectrometer was externally calibrated by use of a Fullerite mixture (Sigma). All spectra were acquired at a laser intensity near the desorption threshold to minimize aggregate formation. The mobility ( $K$ ) of a swarm of ions is defined as the ratio of the ion drift velocity ( $v_d$ ) to electric field ( $E$ ), i.e.,  $v_d = KE$ . The ion drift time ( $t_d$  = length of the drift cell/drift velocity) is inversely proportional to  $K$ , as described by McDaniel and Mason.<sup>28</sup> The drift time ( $t_d$ ) is determined by measuring the mean arrival time distribution (ATD =  $t_d + t_0$ , where  $t_0$  is the time ions spend outside the drift cell) at the detector as a function of the applied voltage ( $V$ ) across the drift cell. The slope of a plot of ATD vs  $1/V$  is inversely proportional to the mobility  $K$  and has an intercept of  $t_0$ . Reduced mobility values ( $K_o$ ) are obtained by scaling the mobility values ( $K$ ) to atmospheric pressure and ambient temperature.<sup>28</sup> A peak picking algorithm (developed by Ionwerks) that takes into account the instrument nominal IM and MS resolutions was used to determine the number of components from the two-dimensional IM/MS plots. In particular, the nominal IM and MS resolutions were determined from experimental measurements of known standards (e.g., Fullerite mixtures).

Atmospheric-pressure photoionization (APPI) mass spectra were obtained with either a low-resolution linear ion trap (LTQ MS) or an ultra-high-resolution 9.4 T FTICR mass spectrometer at the National High Magnetic Field Laboratory, as previously described in detail.<sup>29</sup> The LTQ mass spectrum provides an independent verification of the molecular weight distribution so that FTICR MS parameters can be optimized to span the most abundant ions in that distribution. Ion source parameters were optimized to the low  $m/z$  range (250 <  $m/z$  < 450) for more direct comparison to the LDI/IM/MS results. Samples were diluted to a final concentration of 500 µg/mL in toluene before flowing through a fused silica capillary at a rate of 50 µL/min into a heated

- (28) McDaniel, E. W. *Mobility and Diffusion of Ions in Gases*; John Wiley and Sons, Inc.: New York, 1973.
- (29) Purcell, J. M.; Hendrickson, C. L.; Rodgers, R. P.; Marshall, A. G. *Anal. Chem.* **2006**, *78*, 5906–5912.

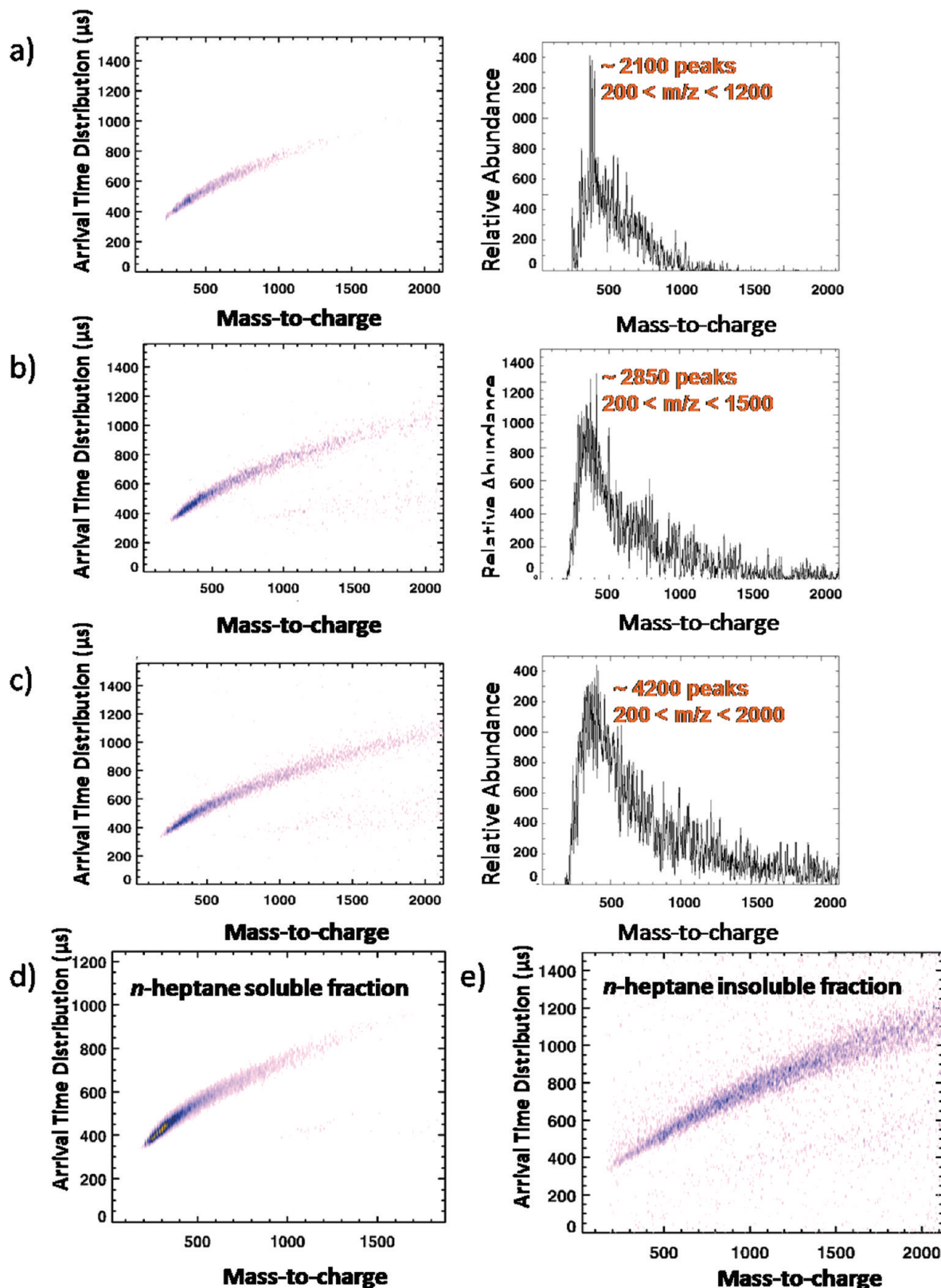


**Figure 2.** Two-dimensional IM/MS and MS projection plots for (a) a light crude oil from Calvert, (b) a medium crude oil from Duri, and (c) a heavy crude oil from San Andro. (d,e) Two-dimensional IM/MS plots for the *n*-heptane-soluble and -insoluble fractions, respectively, of the San Andro heavy crude oil.

vaporizer chamber where nebulization occurred with  $N_2$  gas at 250 °C. The sample then passed in front of a vacuum ultraviolet krypton lamp where photoionization occurred, after which ions were swept into the first pumped chamber of the mass

spectrometer. Our main focus is the elemental composition of ions with  $250 < m/z < 450$ . Ionization and ion accumulation parameters were optimized for the low mass range, resulting in molecular weight distributions in the range  $250 < m/z < 750$ .

### Calvert light crude oil

FT-ICR MS at 9.4 Tesla  
8,482 peaks > 6σ; 250 < m/z < 750  
m/Δm<sub>avg</sub> = 600,000 at m/z = 550

300 400 500 600 700 800  
m/z

### Duri medium crude oil

FT-ICR MS at 9.4 Tesla  
11,852 peaks > 6σ; 250 < m/z < 750  
m/Δm<sub>avg</sub> = 600,000 at m/z = 550

300 400 500 600 700 800  
m/z

### San Andro heavy crude oil

FT-ICR MS at 9.4 Tesla  
15,841 peaks > 6σ; 250 < m/z < 750  
m/Δm<sub>avg</sub> = 600,000 at m/z = 550

300 400 500 600 700 800  
m/z

**Figure 3.** Broadband positive-ion APPI FTICR mass spectra for three crude oils.

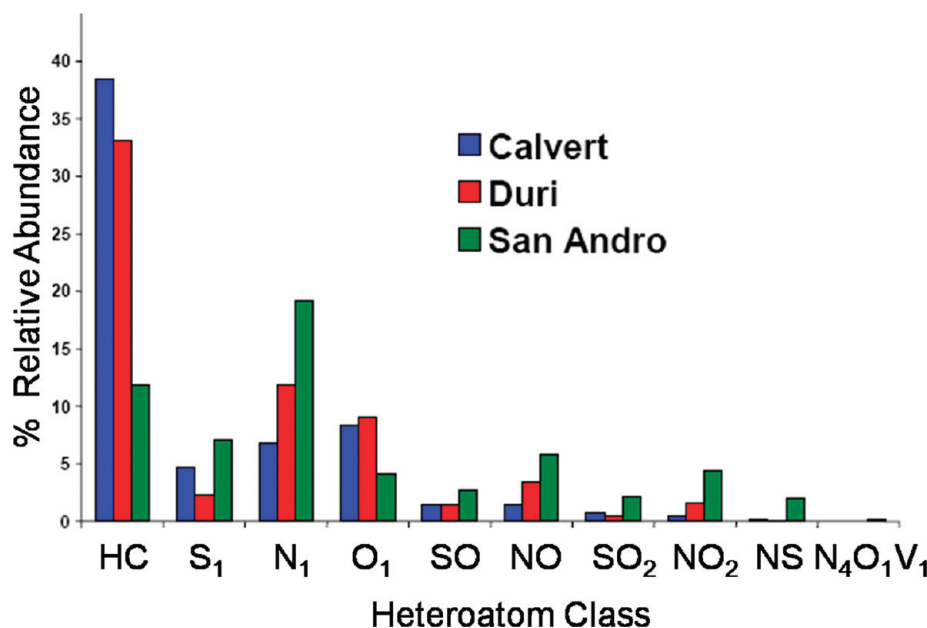
## RESULTS AND DISCUSSION

In IM/MS, IM introduces an additional post-ionization separation prior to mass analysis, thus providing an inherent increase in the peak capacity of any mass spectrometer. At the same time, IM provides complementary information on the composition and

gas-phase packing density (or mobility,  $K$ ) that can validate candidate structures. To illustrate the effectiveness of the IM/MS approach in the analysis of petroleum crude oils, three samples were studied: a Calvert light crude oil, a Duri medium crude oil, and a San Andro heavy crude oil. Two-dimensional IM/MS plots for the three samples are displayed in Figure 2a–c, and the *n*-heptane-soluble and -insoluble fractions of the San Andro heavy crude oil are shown in Figure 2d and e, respectively. In proceeding from light to medium to heavy, the molecular weight distribution shifts to higher  $m/z$  values (Figure 2a–c, right), namely, from  $200 < m/z < 1200$  (~2100 peaks) to  $200 < m/z < 1500$  (~2850 peaks) to  $200 < m/z < 2000$  (4200 peaks), respectively. In particular, the *n*-heptane-soluble fraction of the San Andro heavy crude oil has a lower and narrower mass distribution ( $200 < m/z < 500$ ), centered at  $m/z = 300$ , than does the *n*-heptane-insoluble fraction ( $500 < m/z < 2000$ ).

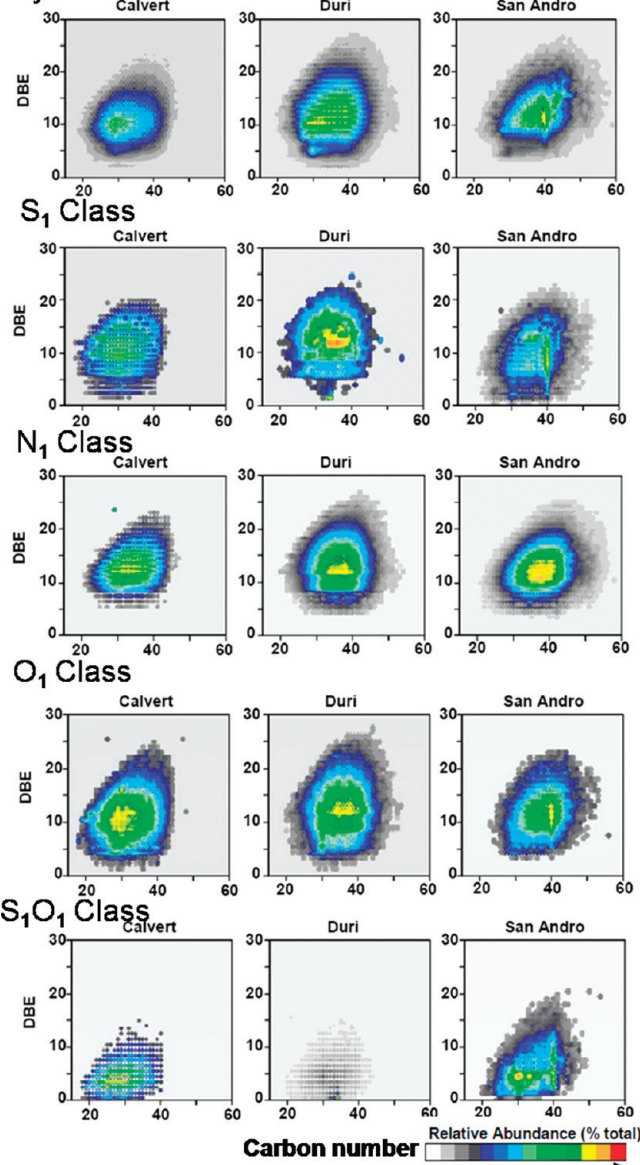
Figure 3 displays positive-ion APPI broadband FTICR mass spectra for the Calvert, Duri, and San Andro crude oils. As for the LDI/IM/MS data, the molecular weight distribution shifts to higher mass in proceeding from light to medium to heavy crude oil. Moreover, ultra-high-resolution MS resolves and identifies the elemental composition (or chemical formulas) of thousands of individual species in each sample. All of the peaks correspond to singly charged ions, based on the unit  $m/z$  separation of  $^{12}\text{C}_n$  and  $^{13}\text{C}_n$  isotopomers of the same chemical formula.<sup>30</sup>

Figure 4 shows the heteroatom class distributions for all three crude oil samples. The Calvert and Duri crudes had the highest relative abundances of hydrocarbon species ( $\text{C}_n\text{H}_n$  series), whereas the San Andro crude was most abundant in  $\text{N}_1$  species ( $\text{C}_n\text{H}_n\text{N}_1$  series). For the Calvert and Duri oils, the  $\text{N}_1$  class was the next most abundant, followed by the  $\text{S}_1$  class ( $\text{C}_n\text{H}_n\text{S}_1$  series). Generally, the heteroatom class relative abundances increase in proceeding from light to heavy crude oils. In agreement with results for other crude oils, vanadyl porphyrins at >1% relative abundance were observed in the heavy San



**Figure 4.** Heteroatom class distributions for Calvert, Duri, and San Andro crude oils.

## Hydrocarbon Class



**Figure 5.** Isoabundance contoured plots of double bond equivalents (rings plus double bonds to carbon) vs carbon number for the hydrocarbon, S<sub>1</sub>, N<sub>1</sub>, O<sub>1</sub>, and S<sub>1</sub>O<sub>1</sub> heteroatom classes.

Andro crude ( $C_nH_hN_4O_1V_1$  series), but not in the lighter Duri or Calvert crude oils.<sup>31–33</sup>

Figure 5 shows color-coded isoabundance contoured plots of double bond equivalents (DBE) versus carbon number for a few heteroatom classes (a description of the procedure to determine the DBE values can be found in refs 5–8). For all three oils, the DBE values of the most stable core structures ranged between 9 and 16. A DBE value of 10 could correspond to three fused polycyclic aromatic hydrocarbon (PAH) rings (e.g., phenanthrene), and a DBE of 14 could correspond to a penta-aromatic

- (30) Senko, M. W.; Beu, S. C.; McLafferty, F. W. *J. Am. Soc. Mass Spectrom.* **1993**, *4*, 828–830.
- (31) Rodgers, R. P.; Hendrickson, C. L.; Emmett, M. R.; Marshall, A. G.; Greaney, M. A.; Qian, K. *Can. J. Chem.* **2001**, *79*, 546–551.
- (32) Qian, K.; Mennito, A. S.; Edwards, K. E.; Ferrughelli, D. T. *Rapid Commun. Mass Spectrom.* **2008**, *22*, 2153–2160.
- (33) McKenna, A. M.; Purcell, J. M.; Rodgers, R. P.; Marshall, A. G. *Energy Fuels* **2009**, *23*, 2122–2128.

core structure (e.g., benzopyrene). For the S<sub>1</sub> class ( $C_nH_hS_1$  series), as for the hydrocarbon class, all three crude oils span similar ranges of carbon number and DBE. For the Duri sample, a DBE of 11–12 is the most abundant, corresponding to benzonaphthothiophene (DBE = 11) or dibenzothiophene with two fused cycloalkane rings (Figure 5). For the N<sub>1</sub> class ( $C_nH_hN_1$  series), carbon numbers ranged between 20 and 50 (lower for the Calvert crude), with a DBE distribution centered between 9 and 12 (Figure 5). A DBE value of 10 could correspond to acridine (pyridinic nitrogen), and a DBE of 9 could correspond to a carbazole (pyrrolic nitrogen). The addition of cyclohexane rings to the core structure could account for the wider DBE distribution. For the O<sub>1</sub> class ( $C_nH_hO_1$  series), carbon numbers ranged between ~15 and 45 (lower for the Calvert crude), with a DBE distribution centered between 4 and 22 (Figure 5). A DBE value of 9 could correspond to dibenzofuran, and the addition of cyclohexane rings to the core structure could account for the higher DBE distributions for Duri and San Andro crude oils. For the SO class ( $C_nH_hS_1O_1$  series), carbon numbers ranged between ~17 and 45 (lower for the Calvert crude), with a DBE distribution centered between 4 and 5 (Figure 5).

Closer inspection of the two-dimensional IM/MS plots shows that several components are separated in the IM domain within a single nominal mass (Figure 6). The observed IMS separation in Figure 6 is based on the inherent differences in ion gas-phase structure: for example, more compact, branched, or condensed structures will have lower ATD values. Conversely, ions of the same molecular class but different masses will be separated in the *m/z* dimension. The broad arrival time distribution illustrates the structural diversity of the petroleum samples while highlighting the utility of the IM/MS separation. For homologous members of a single molecular class (such as fullerenes<sup>20</sup> or polymeric molecules<sup>21</sup>), an increase in *m/z* is typically accompanied by a near-linear increase in ATD. This is not the case for crude oils, as shown in the inset of Figure 6 (bottom), indicating a high degree of structural and compositional diversity. Thus, species separated by less than a few millidaltons probably arise from different heteroatom classes, different combinations of carbon number and DBE, or structural isobars. IM/MS yields a 3–5 fold increase in the number of resolved peaks compared to one-dimensional MS separation (Figure 2). Complementarily, FTICR MS yields a 10–100 fold increase in the number of resolved peaks, plus unique elemental composition identification, but it does not in general resolve structural isomers (although it is possible to distinguish five-membered from six-membered nitrogen heterocycles).<sup>34</sup>

Direct measurement of the mobility values requires the determination of the ion *m/z* values to permit the heteroatom class assignment. Nevertheless, by taking advantage of the ultra-high-resolution MS results, some general trends can be determined in the two-dimensional IM/MS plots. For example, the Calvert crude oil presents the largest abundances of the  $C_nH_h$  series, particularly at low *m/z* values (*m/z* < 320), thereby revealing the two-dimensional IM/MS conformational space for this series (Figure 6 (top)). That is, the two-dimensional IM/MS spectrum of the Calvert crude oils is composed of consecutive series of  $C_nH_h$

- (34) Purcell, J. M.; Rodgers, R. P.; Hendrickson, C. L.; Marshall, A. G. *J. Am. Soc. Mass Spectrom.* **2007**, *18*, 1265–1273.

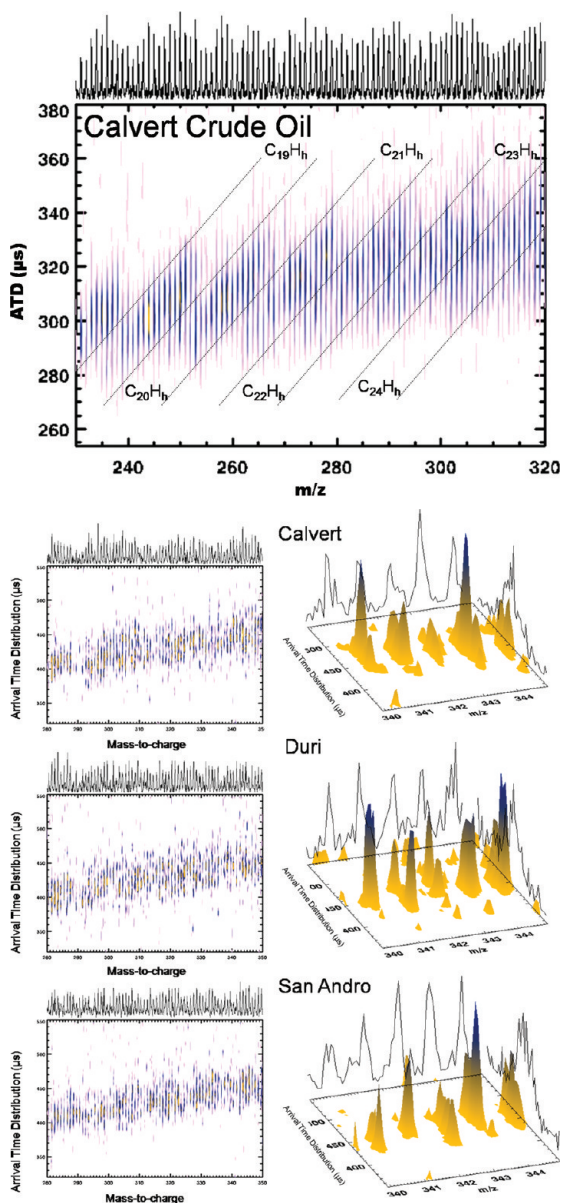


**Figure 6.** (Top) Two-dimensional IM/MS plot for the  $C_nH_h$  series of Calvert crude oils for  $n = 19, 20, 21, 22, 23$ , and  $24$ . (Bottom) Two-dimensional IM/MS and three-dimensional IM/MS plots of the  $280 < m/z < 350$  and  $340 < m/z < 344$  regions of the Calvert, Duri, and San Andro crude oils. Note the unique compositional pattern in the two-dimensional IM/MS plots and the separation in ATD for species of the same nominal mass in the three-dimensional IM/MS plots.

ions: for a given  $C_n$  value, the ATD increases linearly with the number of hydrogen atoms ( $h$ ). The FTICR MS data show that the relative abundances for the various  $C_nH_h$  series distribute normally about a central C/H ratio of 1:1.44. The number of hydrogen atoms ( $h$ ) for a given carbon number ( $n$ ) increases with  $m/z$ , with  $h \approx 12-40$  in the  $200 < m/z < 600$  range. For other heteroatom classes  $C_nH_hXY$  ( $XY = N_1, S_1, N_1, O_1, NS, SO_{1-2}, NO_{1-2}$ , etc.), the heteroatom trend lines can overlap in the two-dimensional IM/MS plot, leading to a more complex ATD and making the identification of individual classes more difficult, as for the San Andro heavy crude oil (Figure 6 (bottom)). Inspection of the ATD and  $m/z$  regions within which unambiguous class assignments allows for the estimation of the relative ordering of the heteroatom classes: as a general trend,

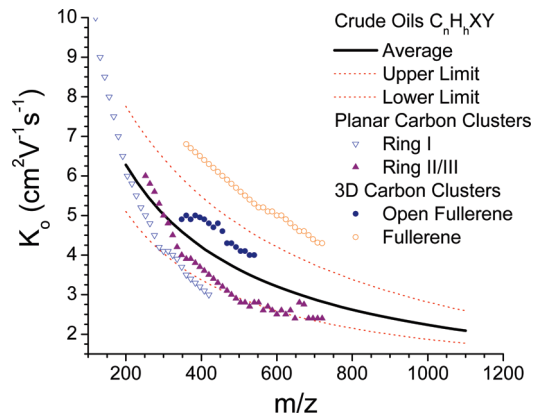


**Figure 7.** Values of the average reduced mobility,  $K_0$ , for the pure ( $C_nH_h$ ) and mixed ( $C_nH_hXY$ ,  $XY = N_1, S_1, N_1, O_1, NS, SO_{1-2}$  and  $NO_{1-2}$ ) hydrocarbon classes. For comparison,  $K_0$  values for various carbon clusters are also included.

the ATDs of the more abundant heteroatom classes are distributed as  $C_nH_h > C_{n-1}H_hN_1 > C_{n-1}H_hO_1 > C_{n-2}H_hN_1O_1 > C_{n-2}H_hS_1$  in the same  $m/z$  range. Note that, although some series might be single-class at lower  $m/z$  values, multiple-class series begin to dominate at higher  $m/z$ , precluding unambiguous heteroatom class assignments.

Figure 7 displays average reduced mobility ( $K_0$ ) values and the upper and lower limits for the observed heteroatom classes. For comparison,  $K_0$  values for planar (i.e., rings I, II, and III) and three-dimensional (i.e., open and closed fullerenes) carbon clusters obtained from previously proposed structures are also shown.<sup>19,35</sup> The reduced mobility values show that, as  $m/z$  increases, the crude oils change from planar to nonplanar structures. At lower  $m/z$ , the mobility values of the pure planar carbon structures coincide with the average values for the crude oils; however, as  $m/z$  increases, the pure planar carbon mobility values shift to the lower limit for the petroleum crude oils. The simplest explanation is that the higher-molecular-weight crude oil species represent noncovalent aggregates, rather than extended planar fused hydrocarbon rings, consistent with a large body of other measurements.<sup>9</sup>

## CONCLUSIONS

Chemical fingerprinting of petroleum crude oil is extremely demanding because the huge number of chemically distinct components requires ultra-high-resolution separation techniques. It is important to note that IM/MS and FTICR MS achieve rapid separation without wet chemical prefractionation. IM/MS offers a 3–5 fold increase in separation compared to one-stage low-resolution MS analysis and can identify the most abundant heteroatom classes. Complementary FTICR mass analysis resolves and identifies all elemental compositions, to enable sorting and interpretation by heteroatom class, double bond equivalents, and carbon number.

Reduced mobility results show that higher-mass components of petroleum crude oils result from noncovalent aggregation rather than planar structures resulting from additional fused rings. Candidate structures for the different heteroatom classes can be validated by their comparison with the reported reduced mobility

(35) Fernandez-Lima, F. A.; Ponciano, C. R.; da Silveira, E. F.; Nascimento, M. A. C. *Chem. Phys. Lett.* **2006**, *426*, 351–356.

values. An anticipated 3–4-fold increase in IMS resolution (currently ~25–40) should permit the determination of the reduced mobilities for the main heteroatom classes. The combination of size/shape speciation by IM/MS and chemical speciation by FTICR MS constitutes a significant advance in fast screening methods for fingerprinting petroleum crude oils.

#### **ACKNOWLEDGMENT**

This work was supported by the Robert A. Welch Foundation (A-1176); the U.S. Department of Energy, Division of Chemical

Sciences, BES (DE-FG-04ER-15520); the NSF Division of Materials Research through Grant DMR-06-54118; and the State of Florida.

Received for review July 17, 2009. Accepted October 30, 2009.

AC901594F